

CFD Modeling of Bluff-Body Stabilized Premixed Flames with Data Assimilation

Yijun Wang*, Sean Walters [†], Nathaniel Overton-Katz [‡], Stephen Guzik[§], and Xinfeng Gao[¶], *Computational Fluid Dynamics and Propulsion Laboratory, Colorado State University, Fort Collins, CO, 80523, USA*

In this work, we focus on investigating the impact of data assimilation on CFD modeling of complex fluid dynamics in a more realistic geometry. The maximum likelihood ensemble filter (MLEF) method is applied due to its advantages for applications to large-scale, nonlinear dynamical systems. The data assimilation impact on the predictability is firstly investigated using the three-dimensional non-premixed Methane-Oxygen flame in a double-shear layer flow configuration. The methodology is then tested for the predictability of flow dynamics structures in a two-dimensional bluff-body geometry. The initial results are encouraging, and data assimilation demonstrates a promising improvement for CFD modeling of complex fluid dynamics in a realistic geometry. Future work will focus on its application to three-dimensional turbulent flows.

I. Nomenclature

Q	Control vector	h	Time step
O	Observation vector	T_{DA}	Data assimilation frequency
R	Observation covariance matrix	t	Superscripts for the truth
P	Ensemble perturbation matrix	f	Superscripts for the forecast
\mathcal{H}	Observation operator	a	Superscripts for the analysis

II. Introduction

For computational fluid dynamics (CFD) modeling of turbulence and combustion in engineering fluid flows, it is well understood that turbulence modeling is difficult and intricate because of the accuracy of the turbulence models. Since direct numerical simulation (DNS) of turbulence is still not feasible even for today's computing power, Reynolds-averaged Navier-Stokes (RANS) or large-eddy simulation (LES) are commonly used as the practical engineering approaches for turbulent combustion modeling. Nevertheless, the challenge is to predict correctly the interactions between the turbulence, chemical kinetics, and thermodynamics properties of the fluid. For instance, LES is a promising approach, however, the accuracy of its prediction is often significantly influenced by the uncertainties in the subgrid-scale (SGS) models. To improve the prediction accuracy, it is important to understand the uncertainties in the dynamical system, including uncertainties in the physical models, model parameters, initial conditions, boundary conditions, numerical methods etc. Data assimilation (DA) algorithm, developed from the application aspect of Bayes theorem, is the science of combining the observations' uncertainties of the dynamical system with the uncertainties in numerical prediction of the system to obtain a more accurate description of the system. The uncertainty estimate is an intrinsic part of the solution in data assimilation algorithm. Our recent work [1-4] has shown great promise in applying data assimilation to CFD modeling of simplified combustion problems for improved prediction and parameter estimation. The present research is interested in applying data assimilation to improve the CFD predictions of more realistic turbulence and combustion problems. While many different types of DA methods are available, such as the variational method [5, 6] (e.g., three-dimensional variational (3D-Var), four-dimensional variational (4D-Var)), the ensemble method [7, 8] (e.g., ensemble Kalman filter (EnKF), ensemble Kalman smoother (EnKS), square root ensemble Kalman filter, maximum likelihood ensemble filter (MLEF)), and the particle method [9–11] (e.g., particle filter, particle smoother), the MLEF

^{*}Graduate Research Assistant, wyj1990@rams.colostate.edu, Student AIAA Member

[†]Graduate Research Assistant, waltersintherockies@gmail.com, Student AIAA Member

[‡]Graduate Research Assistant, noverton@rams.colostate.edu, Student AIAA Member

[§] Assistant Professor, Stephen.Guzik@colostate.edu, AIAA Member

[¶]Associate Professor, xinfeng.gao@colostate.edu, AIAA Member

method is adopted for its advantages in applications to large-scale, nonlinear dynamical systems. In this study, we extend our existing data-assimilated CFD modeling framework with MLEF to obtain understanding of the predictability of the turbulence and combustion in a bluff-body combustor (BBC) geometry.

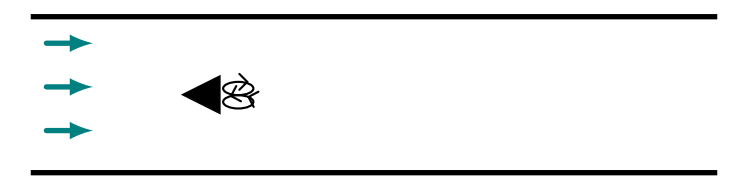


Fig. 1 The schematic of the bluff-body combustor geometry developed by the US Air Force Research Lab (AFRL).

This bluff-body combustor [12], as illustrated in Fig. 1, resembles the practical combusting devices with three core elements including the anchored flame region, the recirculation region, and the mixing shear layer. For the present study, two stages of investigations are carried out in sequential in order to elucidate the assimilation impact on predictability by isolating the complex physics factors. As a starting investigation, we focus on improving the prediction of mixing-layer dynamics with data assimilation. A double shear layer (DSL) non-premixed Methane-Oxygen flame (without wall boundaries) is configured to demonstrate the validity of the data-assimilated CFD algorithm. This simple reaction problem mimics the mixing regions in the BBC as shown by the boxed region in Fig. 2 and helps to assess the performance of the data assimilation for estimating multiple non-observed model states in the coupled dynamical system. This facilitates the building of the framework for future investigations of the turbulent combustion in the BBC geometry. Secondly, the complete domain as shown in Fig. 1 is investigated by focusing on data assimilation impact on the turbulent flow dynamics structures with geometric influence.

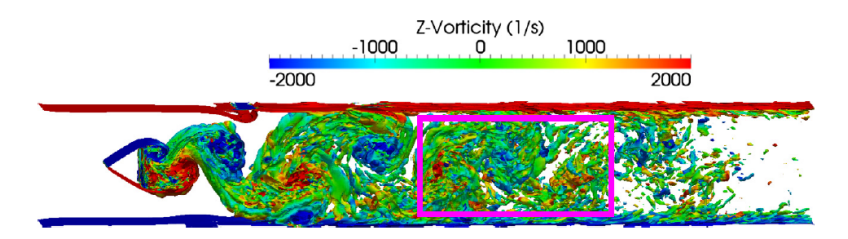


Fig. 2 The iso-surfaces of vorticity magnitude [13].

The organization of this paper is as follow. In section III, we briefly overview the forward model and the data assimilation algorithm, along with the observation quality control, initialization strategy, and quality assessment of data assimilation. The setup of the numerical experiment is detailed in section V. Section VI presents the results to demonstrate the improvement of turbulence predictability with MLEF for two-dimensional BBC cold flows. Concluding remarks and future work are given in Section VII.

III. Algorithms

A. Forward Model: Chord

A fourth-order finite-volume code, Chord [14–18], is used as the forward model. Chord is our inhouse CFD code, designed for achieving high-order accuracy in time and space on modern high performance computing architecture for modeling fluid flows with turbulence and combustion. Chord features adaptive mesh refinement (AMR) in space and time, accommodates complex geometry while preserving free-stream conditions with mapped multiblock technique, and scales to at least 1×10^5 cores. Readers interested in Chord are referred to the above references.

B. Data Assimilation Algorithm: Maximum Likelihood Ensemble Filter (MLEF)

The maximum likelihood ensemble filter [19] (MLEF), one of the ensemble-based data assimilation methods, is implemented and applied to improve the CFD predictions under the circumstances where large uncertainties exist in

initial conditions. In general, MLEF has a theoretical advantage in nonlinear data assimilation problems over standard ensemble methods because it is a straightforward application of standard optimization algorithms developed in control theory, which is suitable for high dimensional nonlinear applications. Briefly, we review the core concept of the MLEF method. Following Bayes formula, one can obtain the posterior probability density function (PDF) from the prior, the conditional, and the observation PDFs. Then, following a general derivation of the cost function under the assumption of the Gaussian PDF (e.g., [20, 21]), the cost function, $J(\cdot)$, is defined as a negative logarithm of the posterior PDF

$$J(\hat{\mathbf{Q}}) = \frac{1}{2} \left[\hat{\mathbf{Q}} - \hat{\mathbf{Q}}^f \right]^{\mathrm{T}} \mathbf{P}_f^{-1} \left[\hat{\mathbf{Q}} - \hat{\mathbf{Q}}^f \right] + \frac{1}{2} \left[\mathbf{O} - \mathcal{H}(\hat{\mathbf{Q}}) \right]^{\mathrm{T}} \mathbf{R}^{-1} \left[\mathbf{O} - \mathcal{H}(\hat{\mathbf{Q}}) \right], \tag{1}$$

where $\hat{\mathbf{Q}}^f$ is the forecast control vector, \mathbf{P}_f is the forecast error covariance matrix, \mathbf{R} is the observation error covariance matrix, \mathbf{O} is the observation vector, and \mathcal{H} is a generally nonlinear observation operator that maps state space to observation space. By minimizing the cost function, MLEF finds the maximum a-posteriori point of the posterior probability distribution that produces a good estimate of the analysis and the uncertainty over the data assimilation intervals.

C. The DA-CFD Framework

In the DA-CFD system, it is critical to couple the CFD and data assimilation algorithms and ensure proper data/information communication between these two components. Chord manages its data based on the structured AMR. When working with complex geometries, such as the case of BBC, Chord employs mapped multiblock techniques to map the physical domain (as shown in Fig. 3a) to the computational one (as shown in Fig. 3b). MLEF uses one-dimensional array for data allocation. In the MLEF-Chord system, the CFD simulation is performed in the computational domain, while the MLEF method calculates the statistical error covariance analysis in the physical domain. Accordingly, a data transfer process is implemented to handle the data communication between Chord and MLEF.

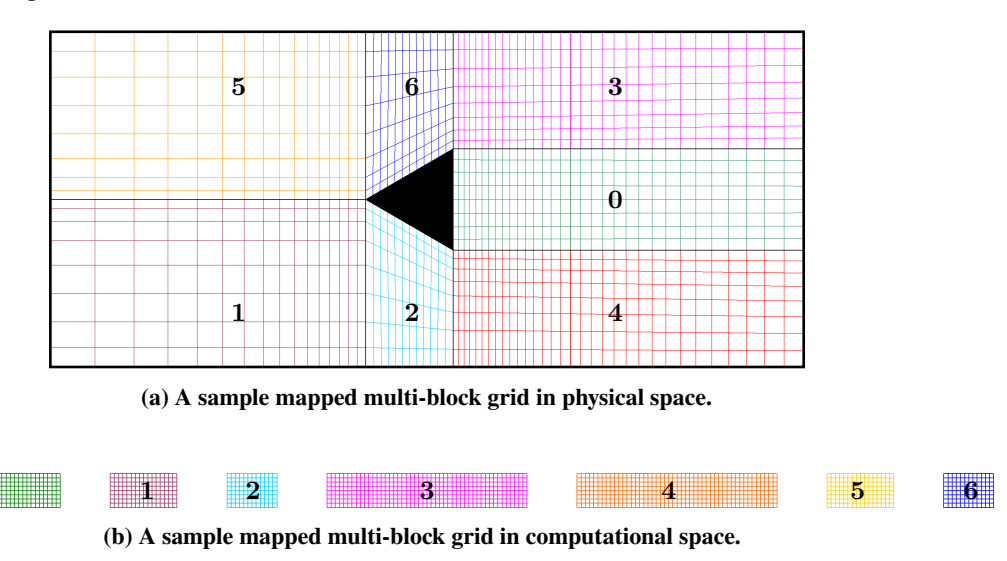


Fig. 3 A sample conforming mapped multi-block grid. Seven blocks are shown in this example, each with a mapping function from its Cartesian computational grid to the curvilinear one in physical space.

There are three steps in the MLEF-Chord system framework. Firstly, each member in the ensemble is propagated by the forward CFD model to the time when the observation data are available and \mathbf{P}_f is evaluated at that time. Then, the observation operator is employed to map the states to the observation space. The observation increment $\left(\mathbf{O} - \mathcal{H}(\hat{\mathbf{Q}})\right)$ is calculated. The \mathcal{H} is the observation operator for mapping the model state space into the observation space since they are not necessarily the same. For instance, Fig. 4 describes an averaging operation process. Introduce the observation operator to be $\mathcal{H}(\cdot) = \mathbf{G} \cdot \mathbf{A} \cdot \mathbf{S}(\cdot)$. The matrix \mathbf{S} is a nonlinear operators for spatial mapping from three dimensions to two dimensions in state space. The matrix \mathbf{A} is an averaging operation to convert two dimensions to one dimension in state space. The matrix \mathbf{G} maps one-dimensional state space to one-dimensional observation space. Finally, Eq. (1) is

optimized with the Broyden–Fletcher–Goldfarb–Shanno (BFGS) method to achieve an optimal deterministic state ($\hat{\mathbf{Q}}^a$) by

$$\hat{\mathbf{Q}}^a = \underset{\hat{\mathbf{Q}}}{\operatorname{argmin}} \left(J_a(\hat{\mathbf{Q}}) \right) ,$$

which is then used to evaluate the square-root analysis error covariance matrix $(\mathbf{P}_a^{1/2})$. To complete the process, all members are updated by using the $\mathbf{P}_a^{1/2}$ and $\hat{\mathbf{Q}}^a$, which initializes the next DA cycle. Our recent work [22] provides a greater detail.

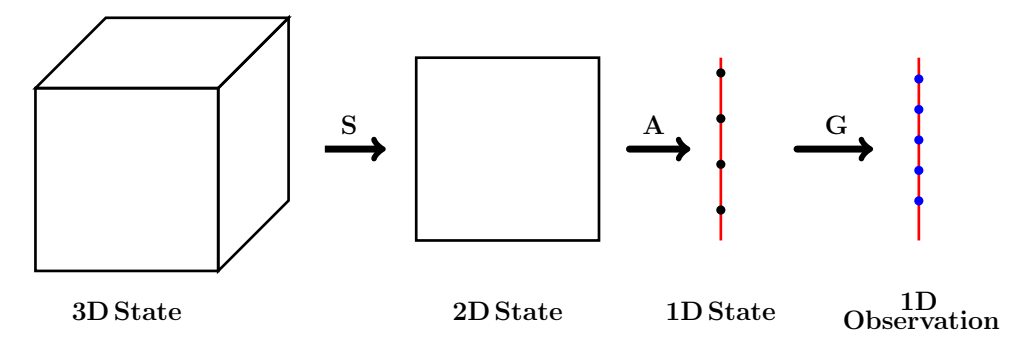


Fig. 4 The schematic of the observation operator, $\mathcal{H}(\cdot)$.

IV. Performance Measures and Strategies

The quality of available information plays an important role in assimilation performance and computational efficiency. Furthermore, the selection of ensemble is critical in the study of initial uncertainties. In this section, we provide necessary background on the performance measures and DA initialization strategies.

A. Observation Quality Control

In order to inspect the potential unfavorable impact of data on the MLEF-CFD solution process and the potential computational cost, the quality of the observation data is examined by the measurements, such as, an error of the observational increment during DA cycles. Under the assumption of Gaussian distribution for the uncertainty, the error of the observational increment should also be expected to follow the Gaussian distribution. However, observations may be distant from the predictions by the forward model at certain time and space, which, if assimilated, would increase the computational cost in the process of determining the optimal state by the MLEF minimizer while have little impact on the analysis. Therefore, a quality region (marked as red shaded region), as shown in Fig. 5, is specified and used to guide the process by eliminating the large error of the observation increment with some thresholds. For example, observation data are assimilated into the MLEF-CFD system only when the errors fall inside the quality region,

$$-C_T \sigma_{\text{obs}} \leq E \left[(\varepsilon_{\text{obs}} - E[\varepsilon_{\text{obs}}])^2 \right] \leq C_T \sigma_{\text{obs}}, \quad \varepsilon_{\text{obs}} \in \left(\mathbf{O} - \mathcal{H}(\hat{\mathbf{Q}}) \right),$$

where $E[\cdot]$ is the expected value in probability theory. The $\sigma_{\rm obs}$ is the standard deviation (SD) of the expected observation error for each model variable, and C_T is the coefficient of the quality control. According to the properties of the Gaussian distribution, 95% of sample that is following the Gaussian distribution falls inside the region of \pm 3SD. Therefore, the C_T is generally set to be 3.0 in the quality control concept. In Fig. 5, only the data inside the yellow shaded region are assimilated.

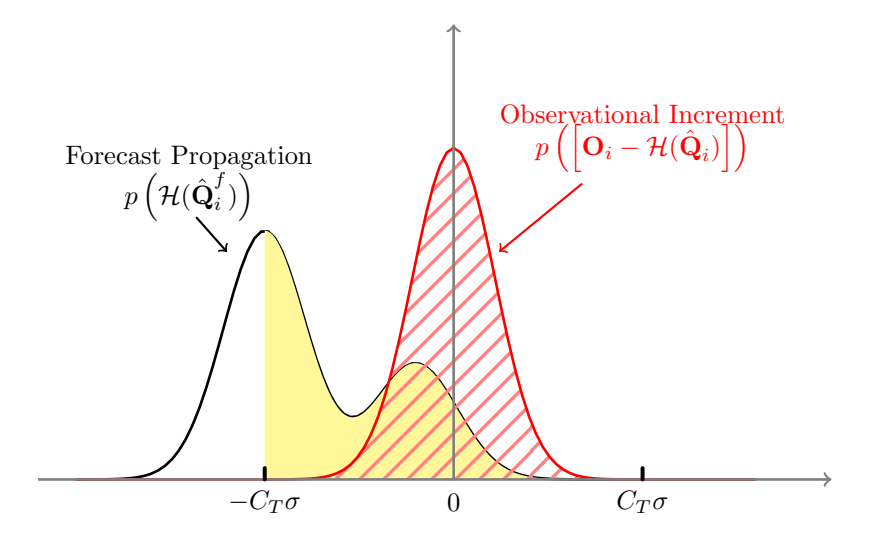


Fig. 5 The schematic of quality control concept used in MLEF method.

B. DA Initialization Strategy

Before any data assimilation can begin, it is necessary to define an initial state and its uncertainty. For initial conditions (ICs) of the assimilation process, the lagged forecast method [23] is used, which typically uses free CFD runs over a time window, $4T_{\tau}$ (usually, $T_{\tau} = T_{DA}$). As shown in Fig. 6, we randomly create N_e unbiased CFD simulations along the $4T_{DA}$ interval, and use those time-lagged predictions to initialize the members (marked as "X") in the ensemble. Moreover, when initializing the deterministic vector $\hat{\mathbf{Q}}_0$ (marked as "A"), the choice can be either selecting a time-lagged run near $t_h = 0$ or simply taking the mean of the initial members in the ensemble. This approach has been used in MLEF with success in the past [7, 19]. Although the perturbations in ICs favor time differences between simulations, some spatial differences are also included as dynamical features are advected over time, so that MLEF is able to recover proper error covariance after only a couple of DA cycles.

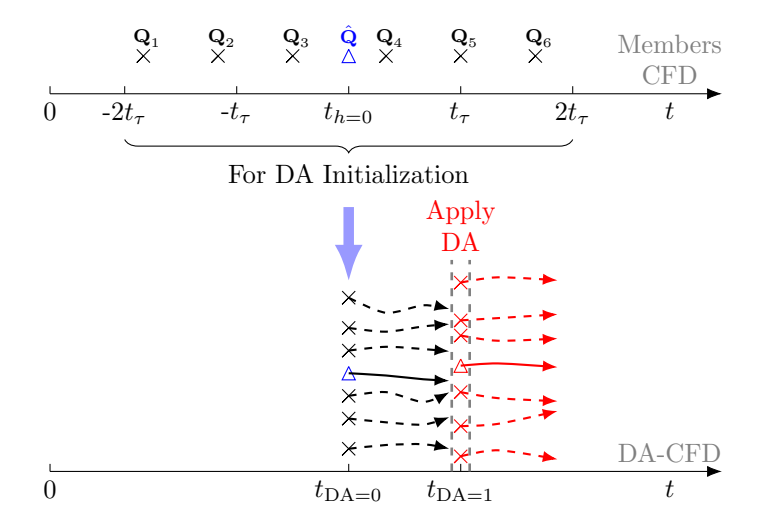


Fig. 6 The schematic of the lagged forecast method.

C. Quality Assessment of Data Assimilation

The data assimilation performance is evaluated by assessing the solution accuracy, the total cost function error reduction, and χ^2 value. Specifically, the error reduction of the total cost function (γ_{tot}) is given by

$$\gamma_{\text{tot}} = \left(\frac{J(\hat{\mathbf{Q}}^f) - J(\hat{\mathbf{Q}}^a)}{J(\hat{\mathbf{Q}}^f)}\right) \times 100\%.$$
 (2)

Since the uncertainty should be reduced after each DA cycle, the total cost function value and error covariance at the analysis stage should always be smaller than the values at the forecast stage. Some large error reduction values are expected at the beginning of DA process. The trajectory along the DA cycles is expected to converge as close to zero as possible. Furthermore, the χ^2 value is calculated by

$$\chi^{2} = \frac{\mathbf{X}^{T}\mathbf{X}}{N_{\text{obs}}}, \quad \mathbf{X} = \left(\mathbf{R} + \mathbf{H}(\hat{\mathbf{Q}})\mathbf{P}_{f}\mathbf{H}^{T}(\hat{\mathbf{Q}})\right)^{-1/2} \left(\mathbf{O} - \mathcal{H}(\hat{\mathbf{Q}})\right). \tag{3}$$

Based on our previous studies, the expected values should be close to 1.0 for cold flows. For a combustion problem, the expected value should be smaller than that of the case without using data assimilation.

V. Numerical Test

A preliminary study of obtaining the solutiondominant covariance interaction of different physical processes is investigated for the assimilation performance assessment using the 3D DSL problem. The configuration of the 3D non-premixed Methane-Oxygen double shearlayer test case is illustrated in Fig. 7. The computational domain is, $L_x \times L_y \times L_z = 137\delta_\theta \times 137\delta_\theta \times 68\delta_\theta$, with triple periodic boundary conditions. The momentum thickness, δ_{θ} , is $\delta_{\omega}/4$, where δ_{ω} is the initial vorticity thickness $(\delta_{\omega} = 0.0005 \text{m})$. Three parallel streams along x-direction are initialized where the center O₂ stream (referred to as stream 2) moves to the left at the root-mean-square velocity of $U_{1,\text{rms}} = 34.03 \text{ m/s}$ with $T_2 = 1350 \text{K}$ and the top/bottom CH₄ streams (referred to as stream 1) move to the right at the same velocity with $T_1 = 300$ K. Two shear layers will develop and reaction will occur as soon as CH₄ mixes with O₂. A 12-species and 38-step chemical mechanism developed by Xu and Wang [24] is used. In

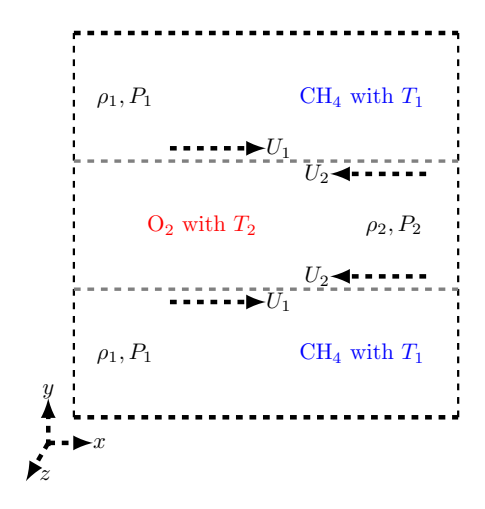


Fig. 7 The schematic of the double shear layer case.

this chemical mechanism, the 12 species are H_2 , H, O_2 , O, OH, HO_2 , H_2O , CH_3 , CH_4 , CO, CO_2 , and CH_2O . The flow has a Mach number of 0.1 based on a velocity equal to the arithmetic mean of the absolute value of the two stream velocities, $U_{1,\text{rms}}$ and $U_{2,\text{rms}}$, a Prandtl number, Pr = 0.71, a specific heat ratio, $\gamma = 1.4$, and a Reynolds number of 11650, based on $Re_{\delta_{\omega},0} = \rho |U_{\text{rms}}| \delta_{\omega}/\mu$ with μ being the Oxygen viscosity ($\mu_{O_2} = 2.02 \times 10^{-5} \text{Pa} \cdot \text{s}$). The hyperbolic tangent profiles are used for initial U(y) and the mass fractions of O_2 and CH_4 . The velocities in each stream are sinusoidally perturbed and computed from a stream function in order to achieve an analytically divergence free initial velocity field.

In this study, all conservative variables are considered to have uncertainties. Twelve members in the ensemble are selected from the lagged-forecast method with setting $T_{\rm DA}=7\times10^{-5}{\rm sec}$ (~9000 time steps). To facilitate the assessment of the assimilation performance, the "observed" components, the mass fraction of the major reactants and the products (CH₄, O₂, CH₃, H₂O, H₂, CO and CO₂), the density, and the x, y and z-momentum, are synthesized by using the perfect solution from the forward model. The present MLEF-Chord system is considered as a "perfect model scenario" by neglecting the forward model error. In addition, for the purpose of better assessing the MLEF performance, free CFD runs (i.e., DA is not applied) are performed to compare with the DA-CFD results and truth.

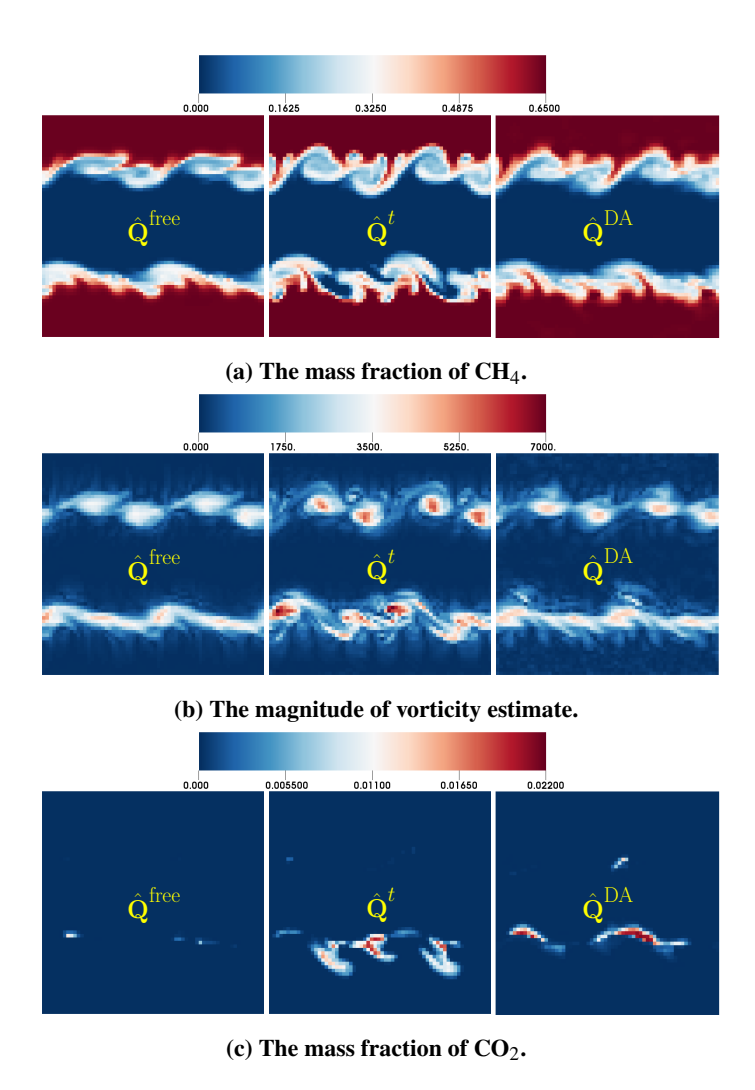


Fig. 8 The solution contour comparison after 5^{th} DA cycle at the middle xy-plane.

The data assimilation performance is firstly assessed by comparing the solution of the model states between the predictions and the truth. The results in Fig. 8 are taken from the DA cycle 5. In each of the subfigures, there are 3 columns, representing the free CFD run, the truth, and the analysis (DA-CFD) from left to right. As shown in Fig. 8a, the mixing of species through convection is captured more sharply in the DA-CFD solution, which appears to have a positive impact on the prediction of CH₄ mass fraction. Furthermore, by comparing the resolutions of the vorticity contours in Fig. 8b, the DA-CFD solution shows increased vorticity magnitude and less dispersion of vortices after 5 DA cycles. When focusing on the vortex cores, the DA-CFD solution is not as dissipated as the free CFD run. Nevertheless, the DA-CFD result is not appreciably improved. Partially, this may be due to the way comparing instantaneous data. Perhaps, comparing some statistical mean data over a characteristic time and/or space region would be more reasonable. Overall, this case demonstrates the interaction between the observed and unobserved quantities in the data assimilation algorithm through the error covariance. Furthermore, this MLEF performance is verified by examining the trajectories of the convergence history of the χ^2 value. By tracking the χ^2 value over the DA cycles and comparing with the free CFD run in Fig. 9, we find that data assimilation is effective in uncertainty reduction because χ^2 of DA-CFD is smaller than that in the free CFD run, as expected. It demonstrates that the data assimilation is implemented properly.

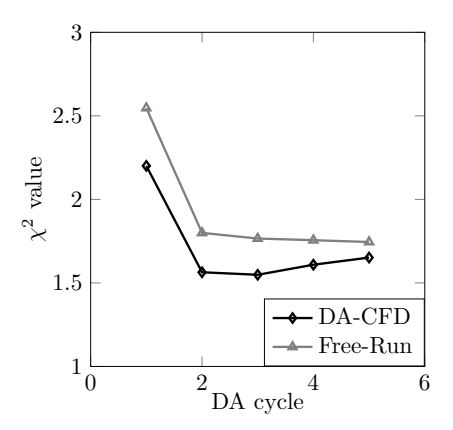


Fig. 9 χ^2 value over the DA cycles.

VI. Results

The MLEF-CFD is applied to the two-dimensional AFRL BBC problem. The computational domain size of the combustor is $L_x \times L_y = 0.829 \text{m} \times 0.127 \text{m}$, with a 38.1mm equilateral triangle flame holder centered in the combustor, as shown in Fig. 10. For the inflow condition on the left boundary, we apply an air inlet velocity of 14.9m/s and an inlet temperature of 310K. The target condition for the total pressure on the right boundary is set to be 100 KPa. No-slip and adiabatic conditions are applied to the top and bottom walls of the combustor as well as the wall of the bluff-body. There are 24 blocks used inside the computational domain, where the minimum mesh size in a single block is 24×16 cells, and the maximum mesh size in a single block is 32×16 cells. The cells are refined near the walls. The stretching ratio in x and y-direction is limited to be less than 10%. The total number of computational cells is 12,032 with the minimal spatial resolution being 4 mm.

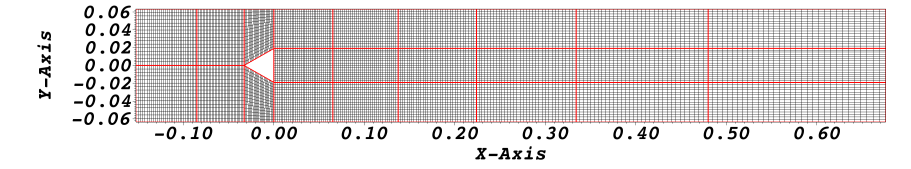


Fig. 10 Computational domain for the two-dimensional AFRL bluff-body combustor.

In this case, we assume all the conservative variables are with uncertainties. There are 19 members in the ensemble created from the lagged-forecast method. The data assimilation frequency is 0.38 flow through time ($T_{DA} = 0.021$ sec). As a reference, a unit flow through time is defined as the total amount of time that a particle travels from the inlet boundary to the outlet boundary along the streamline, which is in form of

1 flow through time =
$$\frac{L_x}{v_{\text{inlet}}} = 0.05564 \text{ sec}$$
. (4)

The "observed" variables are the density, x and y-momentum inside the physical location region of $0 \le x_{loc} \le 0.677$ m and $-0.635 \le y_{loc} \le 0.635$ m. The observations are synthesized by using the "perfect" solution from the forward model

$$\mathbf{O} = \mathcal{H}\left(\hat{\mathbf{Q}}^t\right) + \vec{\eta}, \quad \vec{\eta} \in \mathcal{N}(0, \mathbf{R}), \tag{5}$$

where, the observation errors along the diagonal term of $\bf R$ are set to be 5-8%. Three DA cycles are performed. In addition, for the purpose of better assessing the MLEF performance, free CFD runs are also performed to compare with the DA-CFD predictions and the truth.

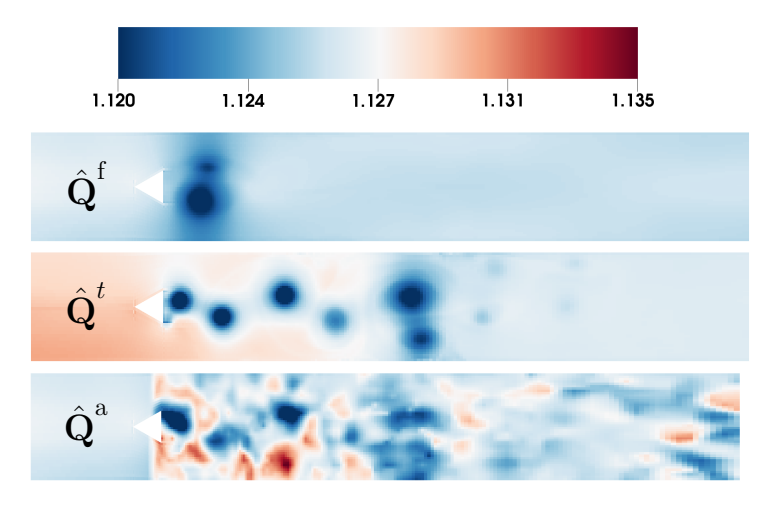


Fig. 11 The ρ contour comparison after 1st DA cycle.

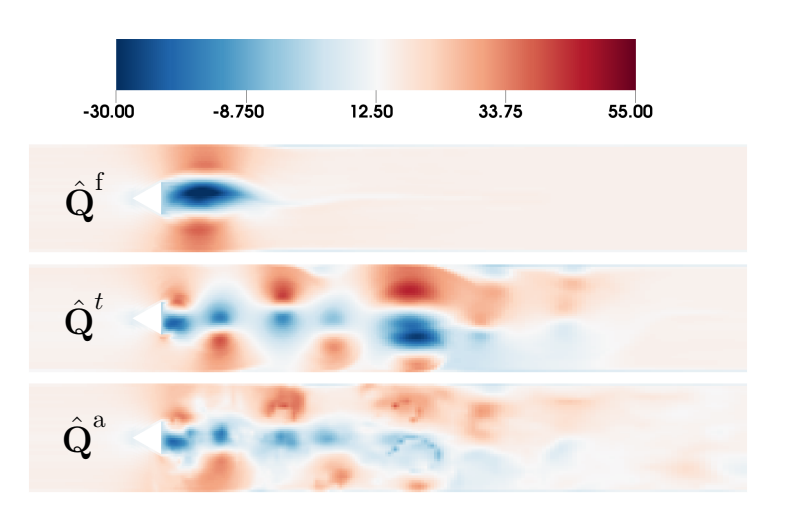


Fig. 12 The ρu contour comparison after 1st DA cycle.

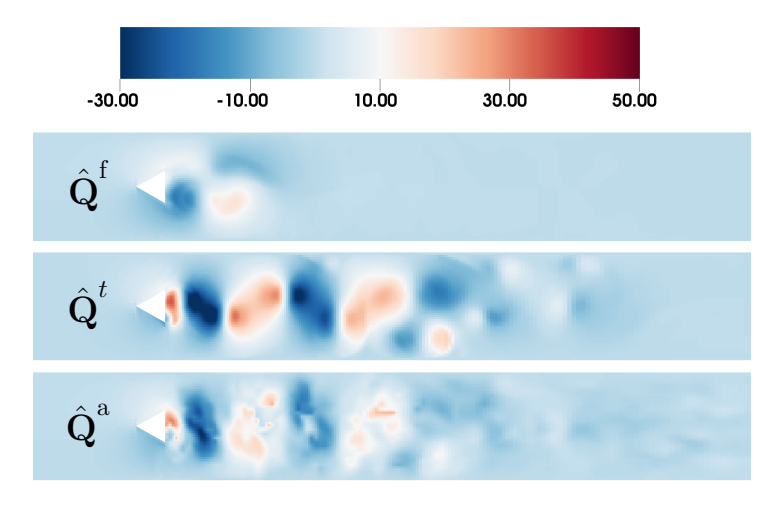


Fig. 13 The ρv contour comparison after 1^{st} DA cycle.

The analysis results after the first DA cycle for the conservative variables, ρ , ρu , and ρv , are compared to the truth and the forecast solutions in Figs. 11-13. In each of the figures, there are 3 rows, representing the forecast, truth, and analysis from top to bottom, respectively. By comparing the contours, we clearly see that the DA-CFD predictions are greatly pulled toward the observations after 1 DA cycle. Without using data assimilation, the velocity fluctuating patterns are completely missed in the free CFD runs. This becomes remarkable in the solutions at the third DA cycle as shown in Figs. 14-17. Specially, when comparing the resolutions of the ρu and ρv contours in Figs. 15 and 16, the downstream portion of the flow structures shown in the analysis contours are getting strongly corrected with the observation information. The free CFD runs do not even produce the correct flow oscillating pattern behind the bluff-body. In general, the analysis results demonstrate that the data assimilation is performed properly.

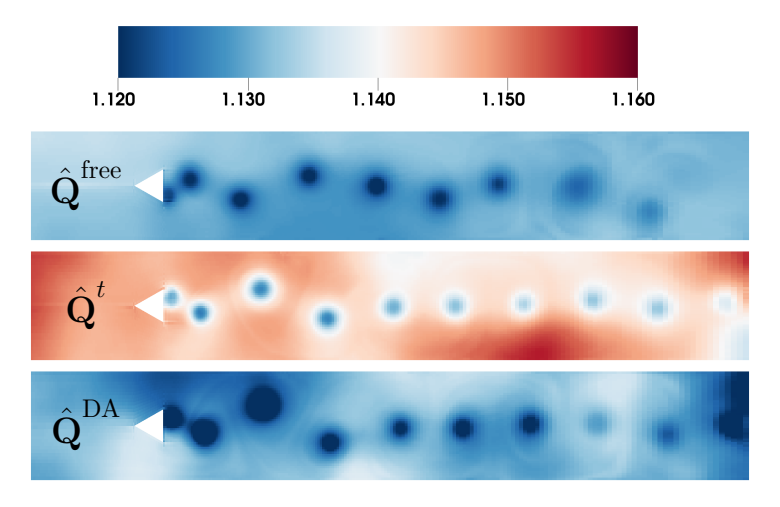


Fig. 14 The ρ contour comparison at 3^{rd} DA cycle.

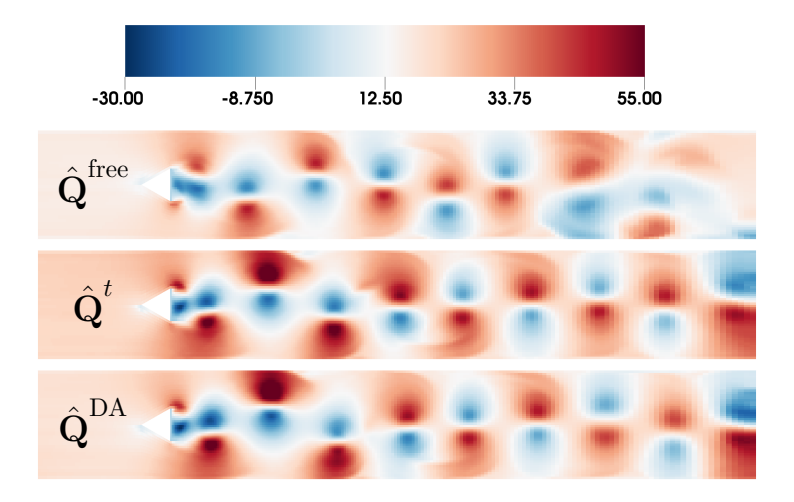


Fig. 15 The ρu contour comparison at 3^{rd} DA cycle.

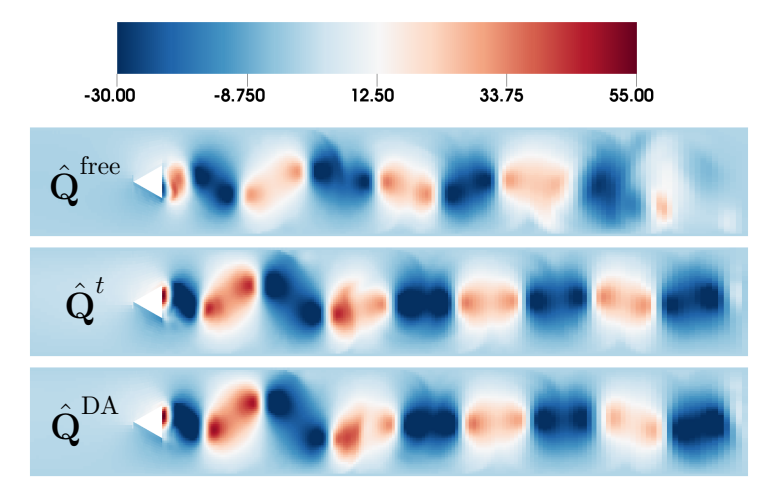


Fig. 16 The ρv contour comparison at 3^{rd} DA cycle.

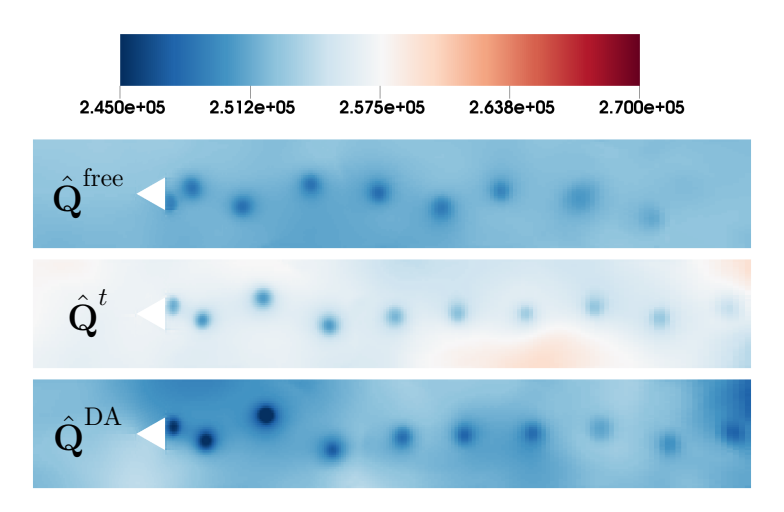


Fig. 17 The energy contour comparison after 3^{rd} DA cycle.

It is worth mentioning that we treat $\rho\epsilon$ as a non-observed variable in the DA-CFD system, and it is expected that the observed data will impact its prediction positively. By comparing the resolutions of the energy contours in Fig. 17, we see that the DA-CFD prediction captures the fluctuating pattern correctly while the free CFD run clearly does not. This improvement is achieved through the coupled dynamics and the solution-dominant covariance between the uncertainties generated in the DA-CFD system.

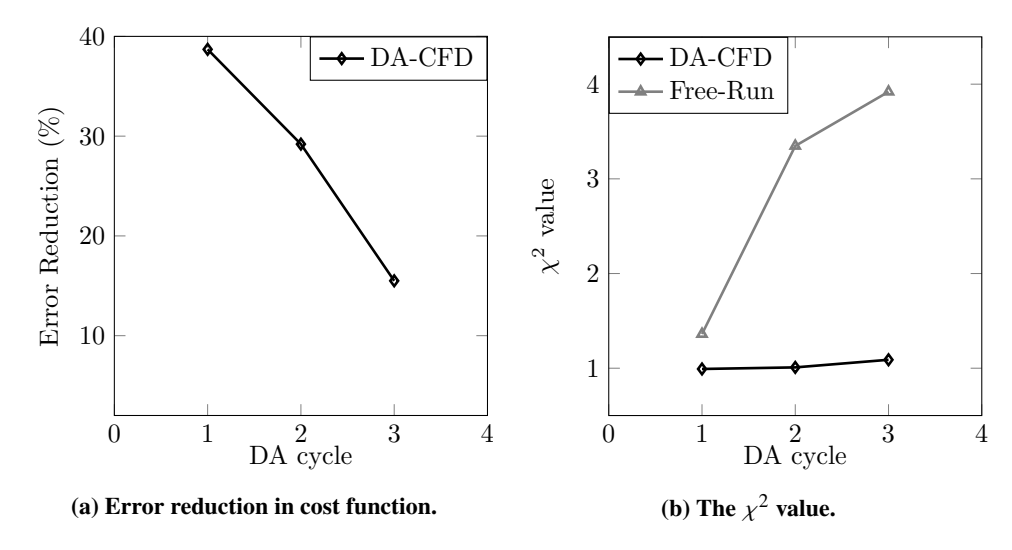


Fig. 18 The total cost function error reduction and χ^2 value.

Moreover, in Fig. 18, we examine the trajectories of the error reduction in the total cost function and χ^2 value for the quality assessment. The trajectory of the error reduction shown in Fig. 18a is clearly consistent with what we have observed above. The overall impact of data assimilating is expected to be decreasing as the DA-CFD predictions converge toward the observations more and more by the DA process. By comparing the χ^2 values along the DA cycles in Fig. 18b, the DA-CFD results are much smaller than the results without using data assimilation, which shows promising uncertainty reduction in the DA-CFD system.

VII. Concluding Remarks and Future Work

Through this study, we have investigated the data assimilation impact on the predictability of flow dynamics structures in a more realistic geometry using MLEF method. Artificial uncertainties are created for the initial conditions, leading to erroneous CFD simulation. This erroneous CFD simulation is then corrected using manufactured observation. The DA-CFD predictions are appreciably improved during the data assimilation process, which demonstrates that the MLEF DA method is a promising tool to improve CFD modeling of complex fluid dynamics when there are data available. Future work will focus on its application to three-dimensional turbulent flows using experimental data for assimilation.

VIII. Acknowledgment

We would like to acknowledge high-performance computing support from Cheyenne (doi:10.5065/D6RX99HX) provided by NCAR's Computational and Information Systems Laboratory, sponsored by the National Science Foundation. This research was supported by Department of Defense United States Air Force (DOD-USAF-Air Force) under the award number FA9550-18-1-0057 and by National Science Foundation under the award number 1723191.

References

- [1] Gao, X., Wang, Y., Overton, N., May, I., and Tu, X., "Estimation of Flame Speed Model Parameter Using Ensemble Kalman Filter Algorithm," *Fall Meeting of the Western States Section of the Combustion Institute*, 2015. WSSCI 2015-134IE-0013.
- [2] Gao, X., Wang, Y., Overton, N., May, I., and Tu, X., "Data Assimilated Computational Fluid Dynamics Algorithm for Combustion," AIAA 2016-1810, 54th AIAA Aerospace Sciences Meeting, 2016.
- [3] Gao, X., Wang, Y., Overton, N., Zupanski, M., and Tu, X., "Properties of a Modified Ensemble Kalman Filter Algorithm for Combustion Application," Tech. rep., 2016. 46th AIAA Fluid Dynamics Conference.
- [4] Gao, X., Wang, Y., Overton, N., Zupanski, M., and Tu, X., "Data-assimilated computational fluid dynamics modeling of convection-diffusion-reaction problems," *Journal of Computational Science*, Vol. 21, 2017, pp. 38–59.

- [5] Talagrand, O., and Courtier, P., "Variational assimilation of meteorological observations with the adjoint vorticity equation. I: Theory." *Journal of the Meteorological Society*, Vol. 113, 1987, pp. 1311–1328.
- [6] Bannister, R. N., "A review of operational methods of variational and ensemble-variational data assimilation," *Q. J. R. Meteorol. Soc.*, Vol. 143, 2016, pp. 607–633.
- [7] Zupanski, M., "Maximum Likelihood Ensemble Filter: Theoretical aspects," Mon. Wea. Rev., Vol. 133, 2005, pp. 1710–1726.
- [8] Evensen, G., Data assimilation: the ensemble Kalman filter, Springer, 2007.
- [9] Doucet, A., de Freitas, N., and Gordon, N., Sequential Monte Carlo Methods in Practice, Springer, New York, 2001.
- [10] Chorin, A. J., and Tu, X., "Implicit sampling for particle filters," Proceedings of the National Academy of Sciences, Vol. 106, No. 41, 2009, pp. 17249–17254.
- [11] Fearnhead, P., and Künsch, H. R., "Particle filters and Data assimilation," Annu. Rev. Stat. Appl., Vol. 5, 2017, pp. 1–31.
- [12] Comer, A., Ihme, M., Li, C., Menon, S., Oefeline, J., Rankin, B., Sankaran, V., and Sankaran, V., "Model Validation for Propulsion Workshop," Accessed online, January 2018. https://community.apan.org/wg/afrlcg/mvpws/p/proceedings.
- [13] Cocks, P. A. T., Soteriou, M., and Sankaran, V., "Impact of numerics on the predictive capabilities of reacting flow LES," *Combust. and Flame*, Vol. 162, 2015, pp. 3394–3411.
- [14] Gao, X., Guzik, S. M. J., and Colella, P., "A Fourth-Order Boundary Treatment for Viscous Fluxes on Cartesian Grid Finite-Volume Methods," AIAA 2014-1277, 52nd AIAA Aerospace Sciences Meeting, 2014.
- [15] Guzik, S. M., Gao, X., Owen, L. D., McCorquodale, P., and Colella, P., "A Freestream-Preserving Fourth-Order Finite-Volume Method in Mapped Coordinates with Adaptive-Mesh Refinement," Comput. Fluids, Vol. 123, 2015, pp. 202–217.
- [16] Guzik, S. M., Gao, X., and Olschanowsky, C., "A high-performance finite-volume algorithm for solving partial differential equations governing compressible viscous flows on structured grids," *Comput. Math Appl.*, Vol. 72, 2016, pp. 2098–2118.
- [17] Gao, X., Owen, L. D., and Guzik, S. M. J., "A Parallel Adaptive Numerical Method with Generalized Curvilinear Coordinate Transformation for Compressible Navier-Stokes Equations," *Int. J. Numer. Meth. Fluids*, Vol. 82, 2016, pp. 664–688.
- [18] Owen, L. D., Guzik, S. M., and Gao, X., "A high-order adaptive algorithm for multispecies gaseous flows on mapped domains," *Comput. Fluids*, Vol. 170, 2018, pp. 249–260.
- [19] Zupanski, M., Navon, I. M., and Zupanski, D., "The Maximum Likelihood Ensemble Filter as a non-differentiable minimization algorithm," O. J. R. Meteorol. Soc., Vol. 113, No. D20110, 2008.
- [20] Jazwinski, A. H., Stochastic Processes and Filtering Theory, Academic Press, New York, 1970.
- [21] Lorenc, A. C., "Analysis method for numerical weather prediction," Q. J. R. Meteorol. Soc., Vol. 112, 1986, pp. 1177–1194.
- [22] Wang, Y., Guzik, S., Zupanski, M., Tu, X., and Gao, X., "Improving Uncertainty Estimation in Turbulence Modeling With Maximum Likelihood Ensemble Filter,", 2019. Manuscript in preparation for Journal of Computational Physics.
- [23] Suzuki, K., and Zupanski, M., "Uncertainty in solid precipitation and snow depth prediction for Siberia using the Noah and Noah-MP land surface models," Frontiers of Earth Science, 2018, pp. 1–11. https://doi.org/10.1007/s11707-018-0691-2.
- [24] Xu, R., and Wang, H., "A skeletal model for methane oxygen combustion in rocket engines," Stanford University, 2018.